

Original Article

Preparation of phenanthroline-2-carbaldehyde functionalized mesoporous silica nanoparticles as nano-chelator for solid phase extraction of trace metals from wastewater

Khaled M AlMohaimadi^a, Hassan M Albishri^a, Khalid Althumayri^b, Awadh O. AlSuhaimi^{b*}, Belal H. M. Hussein^c

^a Department of Chemistry, Faculty of Science, King Abdulaziz University, Jeddah 21589, 80203, Saudi Arabia

^b Department of Chemistry, Taibah University, Medina Munawarah, 42367, Saudi Arabia

^c Department of Chemistry, Faculty of Science, Suez Canal University, Ismailia, 41522, Egypt

ARTICLE INFO

Keywords:

Dual-templates PEG and CTAC
Functionalized mesoporous silica
Heavy metal adsorption
ICPMS
Nanoparticles
Phenanthroline-2-carbaldehyde
SPE

ABSTRACT

This study reports a facile synthesis for mesoporous silica nanoparticles (MSNs) chemically functionalized with a phenanthroline-2-carbaldehyde (PCA) chelating moiety and explore its potential as an efficient solid phase extraction (SPE) nano chelator for Pb, Cd, Ni, and Co ions from aqueous solutions. MSNs were prepared from a sodium silicate solution serving as a silica source and cetyltrimethylammonium chloride (CTAC) and polyethylene glycol (PEG) as structural directing agents, using a simple hydrothermally assisted sol-gel process. The PCA chelator was chemically anchored onto the MSN surfaces. This was done by straightforward transformation incorporation of an amino group via silylation, followed by amide coupling. The obtained nano chelator was characterized using X-ray diffraction (XRD), field emission scanning electron microscopy (FE-SEM), Fourier transform infrared (FTIR), thermogravimetric analysis (TGA), and Brunauer-Emmett-Teller (BET). The materials exhibited a rapid adsorption rate, and the equilibrium for the investigated heavy metals was achieved within 70 minutes. The ideal pH values for metal extraction were 5 for Cd and Co ions and 6.0 for Pb and Ni. The Langmuir model indicated the highest adsorption capacity of heavy metal ions in this order; Ni (132 mg/g), Co (130 mg/g), Pb (121 mg/g), and Cd (116 mg/g). The nano chelating resin demonstrated adequate applicability as a SPE sorbent to extract the targeted metal ion from wastewater reference material and wastewater real samples followed by quantification with inductively coupled plasma mass spectroscopy (ICPMS).

1. Introduction

Solid-phase extraction (SPE) has long been established as an effective method for sample preparation in the analysis of metal ions and other analytes from diverse sample matrices [1]. A wide range of natural and synthetic adsorbent materials, such as natural zeolites [2], activated carbon, [3] chitosan and its derivatives [4], Amberlite [5], clay minerals [6,7], and fly ashes [8], can be effectively employed to extract and separate metals. In addition, the ability to modify many of these materials with specific reagents could tailor their selectivity to bind certain ions. However, these adsorbents suffer from serious limitations, including heterogeneous structure, irregular pore size distribution, poor selectivity for metals, and restricted adsorption capacity.

Over the past years, the emerging nanomaterials have become more popular in wastewater treatment to remove metal ions and other pollutants due to their high specific surface area, porosity, surface functionalities, and specific binding capabilities [9-11]. The use of nanostructured materials, such as carbon-based, silica-based, metallic, and metal oxide nanoparticles—such as zero-valent iron (ZVI), iron-oxide-based magnetic nanomaterials, and nanocomposites—as nano-adsorbents for the SPE of various analytes, including trace metals [12,13] have attracted increased attention. MSNs exhibit favorable characteristics for metal adsorption applications, notably their large

surface area, consistent pore size distributions, and adjustable pore diameters [14]. The high concentration of silanol groups on the surfaces and within the pores of mesoporous silica nanoparticles (MSNs) result in a hydrophilic surface, facilitating functionalization with specific groups and improving their affinity for target metals [15]. The development of solid-phase nano extraction materials is receiving considerable interest as an environmentally friendly method for analyte extraction and enrichment. This approach offers several advantages, including optimized selectivity and sensitivity, reduced utilization of harmful solvents, and shorter extraction times. The use of advanced sorbents could substantially improve analytical methodologies, producing more rapid and accurate results [16].

Alkylsilane precursors are commonly used in the synthesis process as they give highly uniform and pure MSNs. The synthesis process typically utilizes a sol-gel method, involving hydrolysis and condensation of alkoxy silane precursors in a water-alcohol medium, often catalyzed by either an acid or a base [17-19]. To facilitate the formation of the mesoporous structure, structure-directing agents (SDAs) such as polyethylene glycol (PEG) and cetyltrimethylammonium bromide (CTAB) are incorporated into the reaction mixture. Subsequently, the SDAs are removed by solvent extraction or calcination leaving a mesoporous framework [18-20].

*Corresponding author.

Email address: asuhaimi@taibahu.edu.sa (A. O AlSuhaimi)

Received: 10 October, 2024 Accepted: 15 December, 2024 Epub Ahead of Print: 10 March 2025 Published: ***

DOI: 10.25259/AJC.79_2024

The high cost of alkoxysilane precursors and their ecological hazards make sodium and potassium silicate solutions preferable precursors. Recent methods have adapted this approach to be more cost-effective and environmentally sustainable [21]. This synthesis combines the established Stöber method with SDAs-templated techniques applied for the synthesis of ordered mesoporous substances (OMS). However, dilute precursors, dispersing agents, and mechanical stirring are used to control particle size and porosity [22-24]. Practically, sol-gel is performed at ambient temperature or med temperature (50–80°C); however hydrothermally assisted sol-gel procedures are gaining an increased popularity because they enable the production of uniform silica nanoparticles, allowing for precise control over size and shape and are easily scalable for industrial applications. Moreover, the hydrothermal process reduces nanoparticle aggregation, enhancing dispersion stability [25-27].

The research on the use of MSNs as nanochelators for the SPE of heavy metals is relatively sparse. However, numerous studies have explored the use of various forms of silica nanoparticles and their composites [12]. For instance, Huang and Hu [28] developed an innovative sorbent comprising magnetic nanoparticles coated with silica (SCMNPs) functionalized with γ -mercaptopropyltrimethoxysilane (γ -MPTMS). This sorbent was employed for the SPE of trace concentrations of Cd, Cu, Hg, and Pb from biological and environmental samples. The extracted metal ions were subsequently analyzed using inductively coupled plasma mass spectroscopy (ICP-MS). Similarly, Shishehbore et al. [29] synthesized a nano-sorbent functionalized with salicylic acid as an immobilized ligand on silica-coated magnetite nanoparticles. This nano-chelator demonstrated potential application as an SPE sorbent for the extraction of Cu, Cd, Ni, and Cr ions from environmental samples. In another study, Rajabi et al. [30] fabricated a novel nano-adsorbent by functionalizing titania/silica nanoparticles with amine groups. The obtained nano sorbent was found to be effective for the preconcentration of Pd, Cu, and Zn ions from water and food samples prior to their analysis by flame atomic absorption spectroscopy (FAAS). Moreover, MSNs modified with triethoxysilyl propylamine were shown to perform effectively as a sorbent for solid-phase microextraction (SPME), facilitating the extraction of Ni ions from water samples via ultrasound-assisted dispersive extraction (USA-SPME) [31]. This material was also applied in an in vitro study for the separation and extraction of Ca ions from blood samples of individuals with chronic kidney disease (CKD) [32]. In addition, thiol-functionalized mesoporous silica-coated magnetite nanoparticles were reported to be an efficient SPE adsorbent for the preconcentration of Cr, Ag, Co, Pb, Zn, and Cu ions from water samples prior to their analysis by FAAS [33]. More recently [34], synthesized a novel nanocomposite chelator by modifying silica nanoparticles with 5-chloro-8-quinolinol, which proved to be highly efficient for the removal and preconcentration of Al ions from various water matrices.

1,10-Phenanthroline (phen) acts as a typical chelating bidentate ligand for transition metals. The compound exhibits an N,N coordinating center and demonstrates the ability to form stable five-membered ring complexes with various metal ions [35]. In a previous study, we devised a silica monolithic chelator by chemically immobilizing the 5-amino-1,10-phenanthroline (5-aphen) moiety within the meso-/micro-porous structure of the monolith [36]. The monolithic chelator exhibited outstanding properties as a miniaturized SPE sorbent. Thus, this study aims to investigate the potential of anchoring the phen derivative, PCA chelator onto high surface area MSNs, which are synthesized from a commercial sodium silicate solution using a hydrothermal-assisted sol-gel method. The proposed functionalization involves PCA coupling through amine condensation. The envisioned MSNs nano-chelator is expected to feature tuned selectivity for the extraction of heavy metals from aqueous solutions and can function as a model solid nano-adsorbent for the extraction/preconcentration of metal ions, particularly Pb, Cd, Ni, and Co, from aquatic environments before their determination with ICP-MS.

2. Materials and Methods

2.1. Materials, apparatus, and instrumentations

The silica source sodium silicate, $\text{Na}_2\text{O}\cdot 3\text{SiO}_2$ (Na_2O , 8%; SiO_2 , 27%) donated by Adwan Chemical Industries Co. Ltd., (Riyadh, KSA). Hexadecyltrimethylammonium chloride (CTAC), polyethylene glycol (PEG 20000), and 3-aminopropyltriethoxysilane (APTES), were acquired from Sigma-Aldrich (St. Louis, MO, USA). The 1,10-Phenanthroline-2-carbaldehyde chelating agent and 001X7 Cation Exchange Resin were purchased from Taiyuan Lanlang Technology Industrial Corp. (Shanxi, China). Ethanol, toluene, hydrochloric acid (37%), nitric acid (69%), ammonium hydroxide (NH_4OH) solution, and stock solutions (1000 mg/L) of cadmium, nickel, cobalt, and lead ions, utilized for the preparation of standard solutions, were purchased from Acros Organics (Geel, Belgium). The pH was adjusted with ammonium acetate buffer (nitric acid was employed to achieve a lower pH). All reagents were of analytical quality and were utilized without any further purification. Water used in all experiments was purified using Milli-Q® Type 1 Ultrapure Water Systems (Merck KGaA, Darmstadt, Germany) and Lab Benchtop Centrifuge Machine, with 100 ml \times 4 Centrifuge from Skyray instruments (Shenzhen, China) was used for separation purposes during material synthesis and adsorption experiments.

The materials were characterized by X-Ray Diffraction (XRD) using a Rigaku Multiflex diffractometer implementing monochromated high-intensity Cu K radiation ($\lambda = 1.54 \text{ \AA}$) (Cedar Park, TX, USA). The N2 adsorption-desorption isotherms and pore characterization was performed with a Micromeritics ASAP 2020 apparatus (Micromeritics, Norcross, GA, USA). The surface areas were calculated using the Brunauer–Emmett–Teller (BET) equation, whereas pore diameters were estimated by non-local density functional theory (NLDFT) based on the distribution's prominent peaks. Pore distributions were determined with the Barrett-Joyner-Halenda (BJH) approach based on the adsorption branches. Images from the (EF)-SEM were obtained using a JEOL 630-F microscope (JEOL Ltd., Tokyo, Japan). An attenuated total reflectance Fourier transform infrared (ATR-FTIR) spectrometer (Thermo Fisher Scientific Inc., Waltham, MA, USA) was used for gathering infrared spectra. The concentration of metal ions was determined using the Agilent Technologies ICP-MS 7500 series (Santa Clara, CA, USA). All instruments were operated in accordance with the manufacturers' standard instructions.

2.2. Preparation of MSNs

The synthesis of MSNs was performed in aqueous solution following our previous hydrothermally assisted sol-gel method exploiting CTAC and polyethylene glycol (PEG) as SDAs (dual template), and ammonium hydroxide as a catalyst [37]. 10 mL of 35% sodium silicate solution was diluted with 50 mL of water before being cycled twice through a cation exchange column to eliminate/reduce the concentration of Na and K ions in the solution. The ion-exchanged solution was slowly added to a 100 mL water solution containing 3 mL of NH_4OH (25% v/v), 1.0 g of PEG, and 15 mL of CTAC (25%) in a hydrothermal vessel. The components were mixed at a constant stirring speed of 300 rpm for 30 mins, then transferred to a hydrothermal autoclave, which was sealed and placed in an oven at 120°C for 12 hrs. The white silica nanoparticle mass was centrifuged, washed with water and ethanol, dried at 100°C for 6 hrs, then sintered at 550°C for 5 hrs to eliminate organic residues.

2.3. Synthesis of PCA-MSNs nano-chelator

The synthesis of PCA-MSNs nanochelator has been attained by chemical attachment of PCA chelating reagent onto the surface and within the mesopores MSNs via post-synthetic grafting to enhance their selectivity for the extraction of transition metal ions. In short, 2 g of MSNs were dispersed in 50 ml of anhydrous toluene under stirring, and 1.25 ml of 3-Aminopropyltriethoxysilane were introduced dropwise. After 8 hours of reflux, the product (MSNs-NH₂) was isolated using centrifugation. The material was subsequently rinsed multiple times with toluene and ethanol and dried in an oven at 70 °C. The dried

MSNs-NH₂ were then dispersed in 50 ml of anhydrous ethanol and 0.6 g of PCA chelator was added and dissolved in the solution. The mixture was refluxed continuously for 24 hours. Subsequently, the solid mass; nano chelator (PCA-MSNs) was separated by centrifuge, washed with ethanol and water, and dehydrated in a vacuumed oven, and kept in desiccator for future characterization and application.

2.4. Adsorption and solid phase extraction experiments

The sorption studies performed to evaluate the sorption capacity, pH effect, and kinetic parameters of the synthesized MSNs chelator were conducted using standard solutions of Pb, Cd, Ni, and Co ions prepared in ammonium acetate buffer at room temperature using batch mode adsorption method. Calculated masses of PCA-MSNs nano-chelators was dispersed in metal solutions in 100 mL centrifuge tubes and agitated to establish equilibrium for the specified time intervals. The mixture was centrifuged at 5000 rpm for 10 minutes to sediment the resin. Subsequently, 5 mL aliquots were pipetted from the supernatant, diluted, and acidified with 5 mL of 2% HNO₃. The unabsorbed concentration of metal ions was determined by ICP-MS and compared to the original concentrations. The sorption capacity of PCA-MSNs chelator for the studied metals was computed using Eq. (1).

$$q_e = \frac{(C_i - C_e)V}{m} \quad (1)$$

In this formula, q_e represents the capacity (mg/g) and V (L) is the volume of the solution. C_i and C_e represent the metal concentrations before and after reaching equilibrium (mg/L), while m (g) is the mass of the PCA-MSNs resin.

The amounts of ions not retained by the chelating resin were used to calculate the adsorption efficiency using Eq. (2).

$$\% \text{ Re} = \left[\frac{C_i - C_e}{C_i} \right] \times 100 \quad (2)$$

For the SPE studies, an identical adsorption method was utilized for standard solutions containing multiple elements of the analyzed ions, reference materials, and wastewater real samples. A washing step to eliminate unchelated ions was performed by carefully withdrawing the supernatant using a pipette. Afterward, the nano-sorbents loaded all with metal ions were redispersed in 2.5 mL of 1.5 M HNO₃ to elute the sequestered metals from the chelator, diluted with deionized water, and analyzed for metal ions using ICP-MS. Standard solutions applied for the generation of calibration curves are produced from multi-element stock solutions and buffered immediately prior to SPE processing.

3. Results and Discussion

3.1. Synthesis and characterization of MSNs and PCA-MSNs

The synthesis of MSNs used in this work was accomplished through sol-gel process using sodium silicate solution as silica precursor in aqueous alkaline media, making use of CTAC surfactant and PEG as dual templates under hydrothermal conditions at 120°C to minimize aggregation and optimize particle size distribution. The synthesized MSNs were calcinated for 5 hrs at 550°C to remove organic residuals. In the Figure 1, the XRD pattern (Figure 1a) confirmed that the synthesized MSNs possess an amorphous structure, although the FE-SEM (Figure 2a) revealed minimally aggregated spherical to cotton ball-like particles with a specific size range from 20 to 45 nm with an average value of 36 nm and a surface area of 1011 m²/g² exhibiting pore size measurements of 3.1 nm. Evidently, the MSN retained its original morphology after washing and post-calcination. Optimization of MSNs synthesis is presented in another article [37].

The MSNs have been used as a substrate for the chemical immobilization of PCA moiety to synthesis MSNs-PCA metal chelator. The chemical attachment of the chelating agent PCA realized via post-synthetic grafting. The chemical functionalization involves two reaction steps as illustrated in Scheme 1. Initially, MSNs were silanized using APTES to yield MSNs-NH₂ intermediate. Subsequently, Schiff

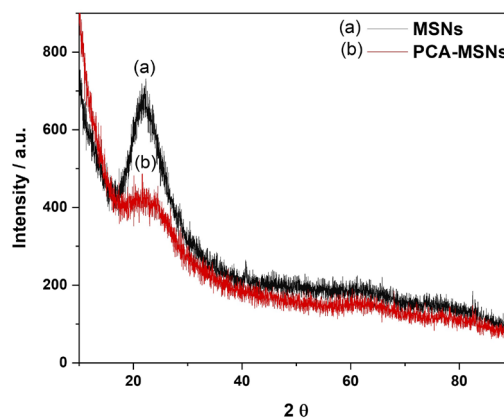
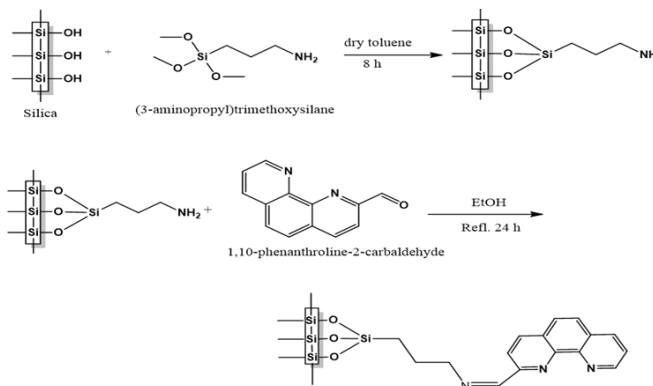


Figure 1. X-Ray Diffraction patterns of plain (a) MSNs and (b) PCA-MSNs.



Scheme 1. Reaction scheme for the covalent attachment of PCA onto mesoporous silica nanoparticles area.

bases are generated through the condensation of MSNs-NH₂ which act as the primary amine, and PCA which has an aldehyde group. The heterogeneous Schiff base enables the selective adsorption of metal ions.

The XRD patterns of the PCA-MSNs confirms that there is no significant change due to the immobilization of the PCA moiety except for the predicted decrease in the XRD peak intensity (Figure 1b). This provides sufficient evidence that the functionalization occurred mainly inside the mesoporous channels indicating that the PCA were evenly dispersed in the mesoporous channels.

The FE-SEM micrographs of unmodified mesoporous MSNs at a 100 nm scale, shown in Figures 2(a) and 2(b), reveal that the mesoporous nanoparticles possess a spherical cotton ball-like morphology featuring minimal aggregation, with average particle sizes of 36 nm for MSNs and 38 nm for PCA-MSNs. The morphology of MSNs is mostly the same after the modification; however, the slight enlargement in particle size could be attributed to the influence of the attached PCA molecules after modification. As seen in Figure 2(b), the modified MSNs demonstrated a noticeable improvement in disparity perhaps due to the attached molecules, which minimize non-specific binding between silica nanoparticles [38]. The modification method seems to have no significant effect on the average particle size of PCA-MSNs (Figures 2c and 2d). The effect of functionalization on surface areas, pore volume, and pore size distributions have been evaluated using nitrogen adsorption-desorption technique. The measurements for MSNs and PCA-MSNs samples were compared. Figure 3 depicts the normal isotherm for the plain MSNs and the PCA modified samples and Table 1 presents the surface area and pore volume. Obviously, all samples exhibit capillary condensation, with P/P₀ values ranging from 0.1 to 0.4. The isotherms exhibit a type IV isotherm, which is characteristic of mesoporous materials. Surface area and pore volume contracted upon the loading of PCA moieties. This is expected as the PCA molecules can be attached to MSNs pores, resulting in reduced pore volume, diameter, and surface.

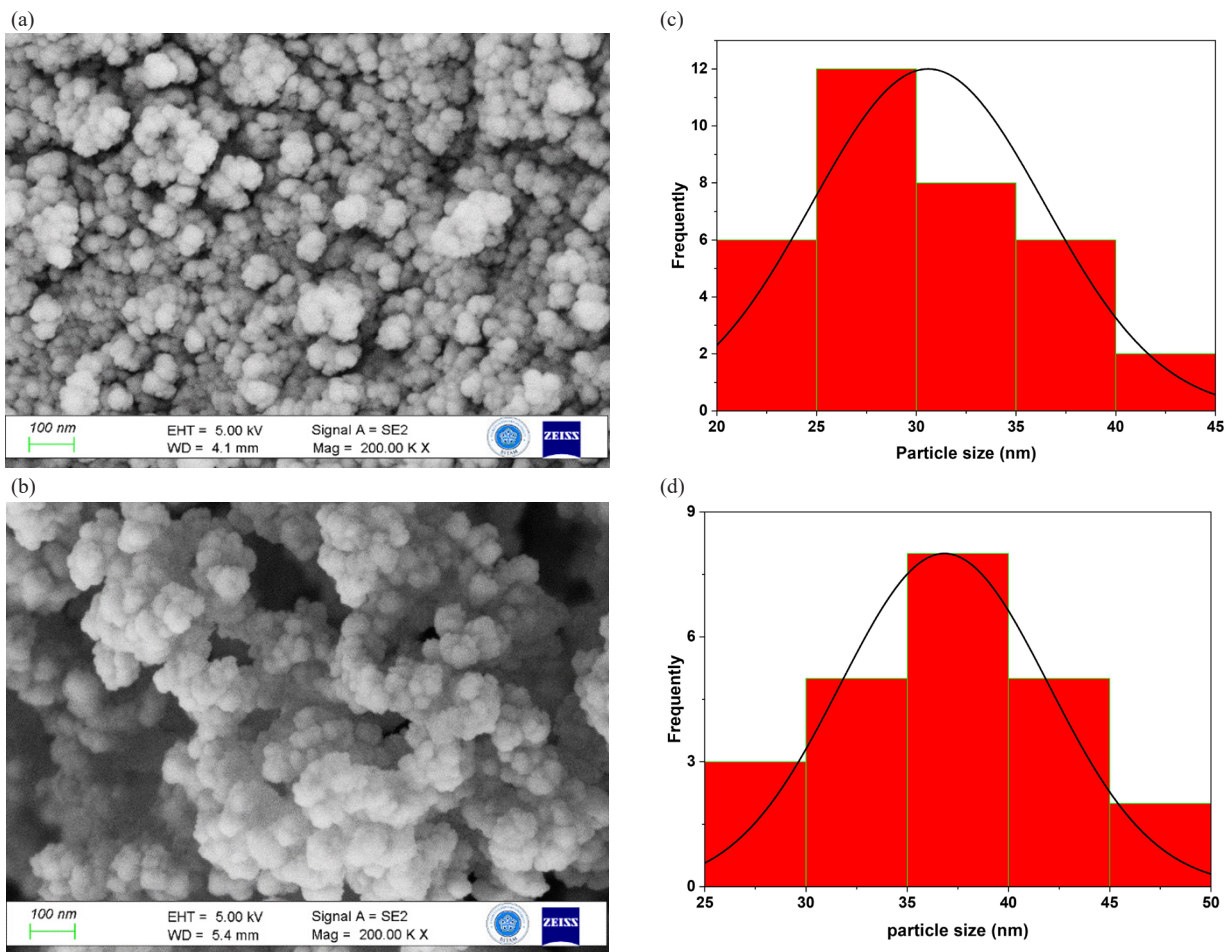


Figure 2. Surface characterization of bare MSNs and PCA-MSNs; (a, c) FE-SEM of bare MSNs and PCA-MSNs; (b, d) the histogram of particle size calculated from FE-SEM.

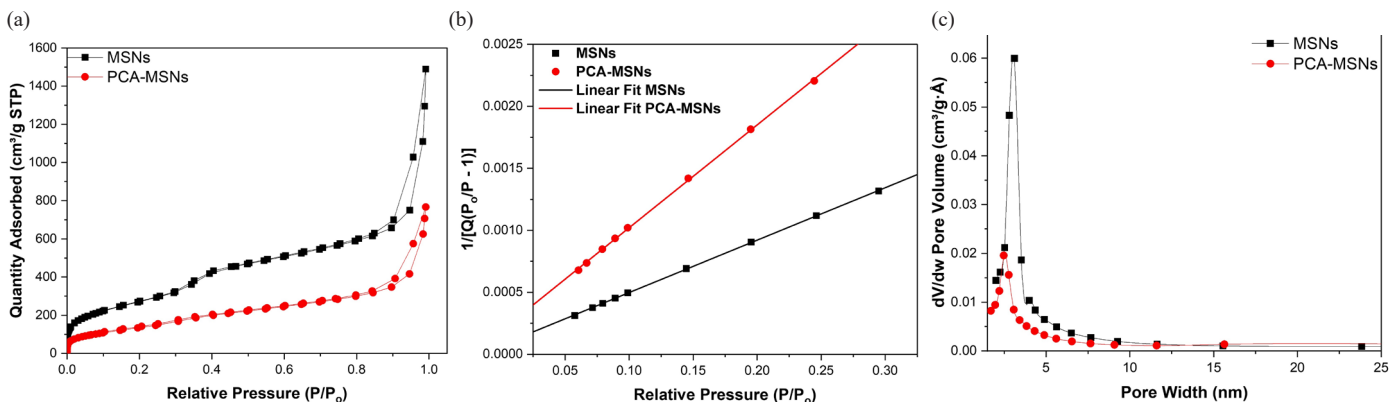


Figure 3. (a) The N_2 adsorption-desorption isotherms, (b) linear, and (c) pore size distribution curves of the MSNs and PCA-MSNs samples.

Table 1. The textural properties of MSNs and PCA-MSNs samples.

Sample	Surface area (m^2/g)	Pore diameter (nm)	Pore volume (cm^3/g)
MSNs	1,011.42	3.11	0.38
PCA-MSNs	512.97	2.4	0.19

Fourier transform infra-red (FTIR) and thermogravimetric analyses were conducted on calcined MSNs prior to and following modification with the chelating agent. Figure 4 illustrates a characteristic FTIR spectrum of calcined MSNs, featuring three distinct bands at 487 cm^{-1} , 608 cm^{-1} , 808 cm^{-1} , and 1088 cm^{-1} . The sharp band at 487 cm^{-1} corresponds to bending vibrations of Si-O-Si, the band at 808 cm^{-1} is ascribed to symmetric vibrations of Si-O-Si, and a broad band at 1088

cm^{-1} is linked to asymmetric vibrations of Si-O-Si in silicon [39]. The FTIR spectra of PCA-functionalized MSNs has broad peaks at $3600\text{--}3100\text{ cm}^{-1}$ and 1627 cm^{-1} , which can be attributed to the stretching or bending vibrations of N-H or Si-OH bands, respectively [40,41]. The absorption signal at 2927 cm^{-1} illustrates the asymmetric stretching of CH_3 due to methyl groups, confirming the effective grafting of PCA onto MSNs.

The thermogram shown in Figure 5 represents the weight loss percentage as the plain MSNs and PCA-MSNs chelator were subjected to a heating program from ambient temperature to 900°C . For temperatures ranging from 25 to 150°C , samples exhibit considerable weight loss due to the loss of adsorbed water. According to [42,43], weight loss below 150°C was caused by water evaporation. Plain silica's

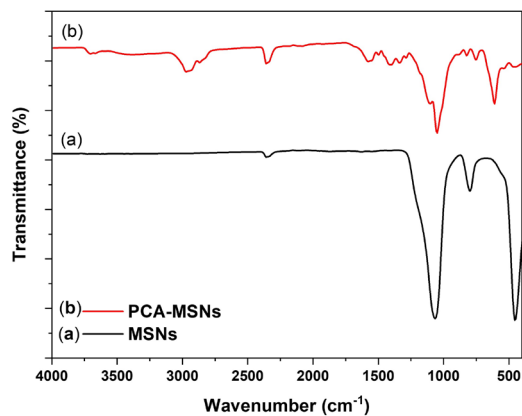


Figure 4. FTIR spectra of MSNs and PCA-MSNs.

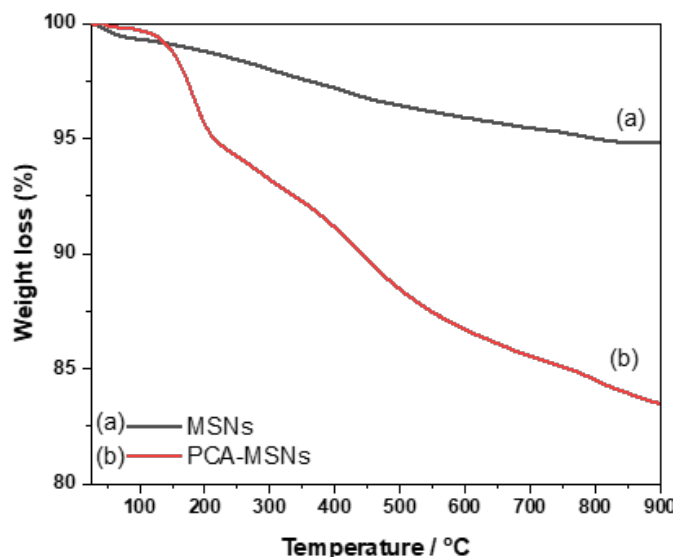


Figure 5. TGA of (a) calcined MSNs at 550°C and (b) PCA-MSNs.

weight remains stable between 180°C and 900°C before a notable gradual mass reduction has been observed. For this temperature range PCA-MSNs, exhibited weight loss due to organic group decomposition, which includes three-step decompositions at 180, 238, and 433°C. The weight reduction for PCA-MSNs was 16.50%, demonstrating that the functionalized PCA ligand decomposes.

3.2. Adsorption studies

3.2.1. Contact time

It is common in the sorption process for rapid adsorption to optimize the operational efficiency of the adsorbent. The adsorption rate is a critical practical factor in the application of SPE adsorbents. Figure 6 illustrates the adsorption rates of Pb, Cd, Ni, and Co ions over different reaction times. Metal ion adsorption occurred rapidly in the beginning, and as contact time increased, the adsorption capacity enhanced but ultimately attained equilibrium. Adsorption equilibrium was unequivocally reached after 45 mins. The characteristics of the adsorbent may elucidate its fast adsorption. The adsorbent might be uniformly dispersed in the aqueous solution. A novel synergistic complexation of Pb, Cd, Ni, and Co ions, along with PCA grafting on MSNs, was observed.

3.2.2. Effect of pH on the adsorption of metal ions

The pH of the solution is a critical factor in achieving a quantitative extraction of metal ions, as it significantly influences the efficiency of

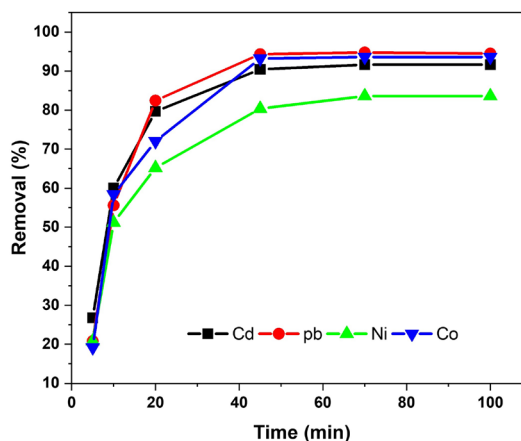


Figure 6. Adsorption efficiency of the metal ion onto PCA-MSNs at different initial metal ion concentrations.

the chelation reaction. This reaction determines the amount of metal ions adsorbed by the chelating resin. The mechanism may involve electrostatic adsorption, ion exchange, or complexation processes. The effect of pH on the adsorption of various metal ions onto PCA-MSNs was investigated over a pH range of 2–9, as shown in Figure 7.

The results clearly indicate that the adsorption capacities of the analyzed metal ions increase significantly with pH in acidic media, reaching maximum values at specific pH levels [44]. This behavior can be attributed to the deprotonation of chelating centers as the pH increased, leading to rise in negative charge and hence facilitating the adsorption of cationic species. However, a further increase in pH resulted in a slight drop in the adsorption capacity of PCA-MSNs, which is more likely due to the formation of metal hydroxyl complexes, that could hinder the complexation of metal ions with the chelating centers on the resin. This effect can also be attributed to the accessibility of active hydroxyl groups, which are abundant on the surface and within the mesoporous structure of PCA-MSNs. Based on these findings, a pH of 5.0 was determined to be optimal for the extraction of Cd and Co ions, while a pH of 6.0 was identified as ideal for Pb and Ni ions.

3.2.3. Adsorption isotherms

The isotherm study is crucial for understanding interactions between adsorbents and adsorbates and provides full knowledge of the adsorption processes. Hence, in this work, the adsorption of Co, Pb, Ni, and Cd ions was carried out at various initial concentrations under pH 5-6 and at a temperature of 298 K as shown in Figure 8. The results indicated that as the initial concentration increased the adsorption capacities of metals. This indicates that the initial concentration ion is critical in pushing raised up ions to move from the liquid to solid phases until maximum adsorption is reached. The adsorption of the studied metal ions by PCA-MSNs represented in Table 1 has been acquired from Langmuir [45] and Freundlich [46] adsorption isotherm models (Eqs. 3-6):

$$q_e = \frac{q_{\max} K_L C_e}{1 + K_L C_e} \quad (3)$$

$$\frac{C_e}{q_e} = \frac{1}{K_L q_{\max}} + \frac{1}{q_{\max}} C_e \quad (4)$$

In this equation, q_{\max} (mg g⁻¹) is the maximum adsorption capacity for the ions. K_L is the Langmuir constant, which directly relates to the energy of adsorption and the affinity of binding sites. Eqs. (5) and (6) define the Freundlich model and its linear representation, respectively:

$$q_e = K_F C_e^{1/n} \quad (5)$$

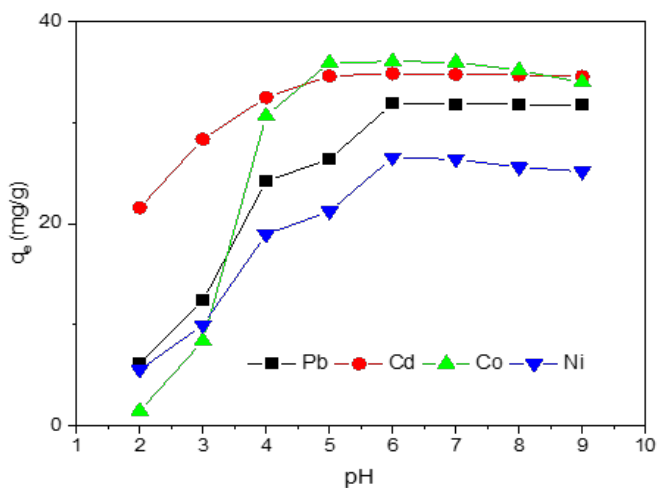


Figure 7. pH dependent on the metal ion adsorptions onto PCA-MSNs.

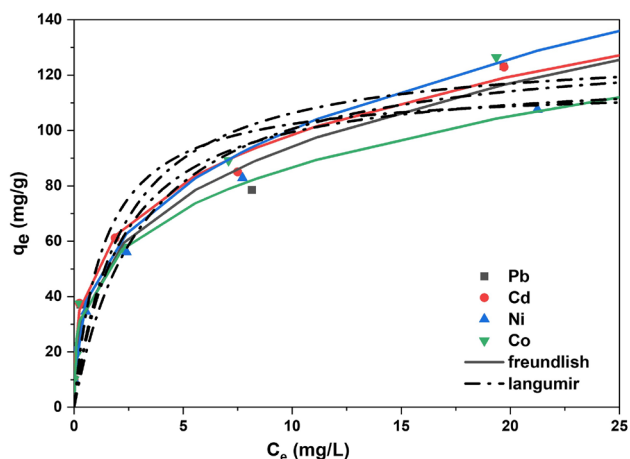


Figure 8. Metal ion adsorption isotherms: Non-linear Langmuir (dashed line) and Freundlich (solid line) isotherms for Pb, Cd, Ni, and Co at different starting concentrations.

$$\ln q_e = \ln K_F + \frac{1}{n} \ln C_e \tag{6}$$

where K_F and n are the Freundlich adsorption constants, showing the adsorption capacity and intensity. It is known that, when the value of $1/n$ falls within the range of 0 to 1, the adsorption process occurs spontaneously [47-49]. The Freundlich curves model (Figure 8)

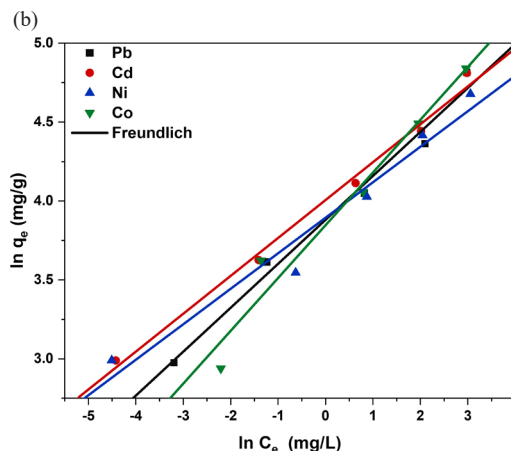
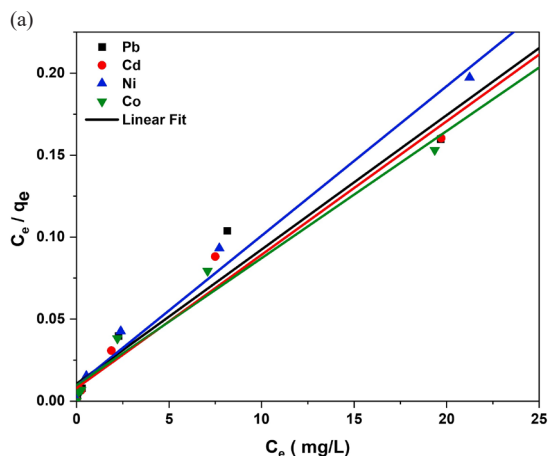


Figure 9. (a) Linear forms for Langmuir isotherm and (b) Freundlich isotherm models of metal ions adsorption onto PCA-MSNs.

demonstrates better correlation coefficients when compared to Langmuir (Figures 9a and 9b), indicating it is the most suitable to describe the adsorption isotherms of the examined metals. The figures display the linear curves of C_e/q_e versus C_e for Langmuir and $\ln q_e$ against $\ln C_e$ for the Freundlich model of the adsorption of metal ions. The values for K_L , q_m , K_F , $1/n$, and correlation coefficients (R^2) from the curves above are provided in Table 2.

The pseudo-first- and pseudo-second-order models were utilized to analyze the kinetics and adsorption data, shown in Figures 10(a) and 10(b). The typical mathematical representation for Lagergren's [50] pseudo-first order rate equation can be expressed by the Eqs. (7) and (8).

$$\frac{d q_t}{d t} = K_2 (q_e - q_t) \tag{7}$$

$$\ln (q_e - q_t) = \ln q_e - n \left(\frac{K_1}{2.303} \right) t \tag{8}$$

In this context, q_t and q_e (mg g^{-1}) represent the adsorption capacity and the equilibrium state, respectively. K_1 (min^{-1}) denotes the rate constant for pseudo-first-order kinetics. Eqs. (9) and (10) define pseudo-second-order interactions [51].

$$\frac{d q_t}{d t} = K_2 (q_e - q_t)^2 \tag{9}$$

$$\frac{t}{q_t} = \frac{1}{K_2 q_e^2} + \frac{1}{q_e} t \tag{10}$$

K_2 denotes the pseudo-second-order rate measured in $\text{g mg}^{-1} \text{min}^{-1}$. (min^{-1}). Table 3 displays the kinetic parameters for the extraction/removal of Co, Cd, Ni, and Pb using PCA-MSNs. The pseudo-second-order model had a higher accuracy (root-mean square error (RSME) < 0.1) than the pseudo-first-order model to predict the adsorption of studied ions, suggesting that the main mechanism is governed by rate chemisorption [52,53].

The intraparticle diffusion model was applied to investigate the sorption reaction's rate-determining phase [54]. The capacity of adsorption was determined using Eq. (11).

Table 2. Langmuir and Freundlich isotherm parameters for Co, Cd, Ni, and Pb adsorption onto PCA-MSNs at 298 K.

Parameter (ions)	q_{\max} (mg/g)	K_L (l.mg^{-1}) $\times 10^5$	R^2	n	k_f ($\text{mg/g}(\text{L/mg})^{1/n}$)	R^2
Pb	121	0.46	0.83	3.21	45.98	0.97
Cd	116	0.75	0.86	3.60	52	0.98
Ni	132	0.32	0.87	3.03	47	0.90
Co	130	0.45	0.92	3.60	45.80	0.93

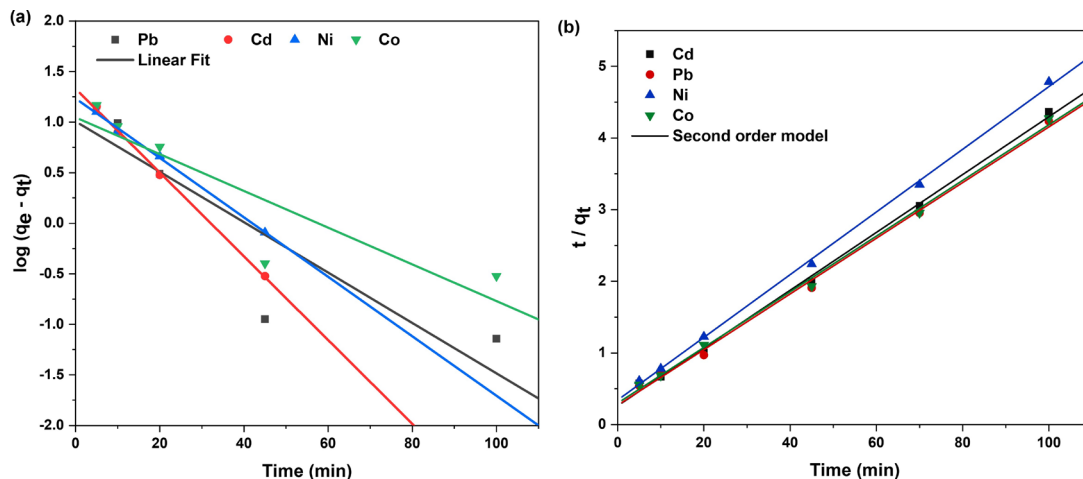


Figure 10. (a) Linear fit of experimental data obtained using pseudo first and (b) pseudo second order kinetic model of metal ion adsorption onto PCA-MSNs.

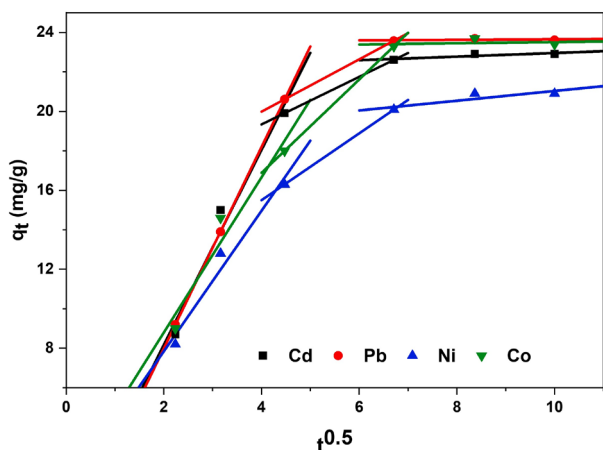


Figure 11. Intersurface diffusion model for adsorption of Pb(II), Cd(II), Ni(II), and Co(II) onto the PCA-MSNs.

Table 3. Kinetic parameters for adsorption of the studied meta ions onto the PCA-MSNs.

	Pseudo second-order model		
	K_2 (g · g ⁻¹ · min ⁻¹) × 10 ⁻³	q_e (mg/g)	RMSE(%)
Pb	1.51	25.73	0.09
Cd	1.63	24.77	0.09
Ni	1.92	22.85	0.06
Co	1.51	25.73	0.09
	Pseudo First-order model		
	K_1 (mg/g · min ^{1/2})	q_e (mg/g)	RMSE (%)
Pb	0.057	10.165	0.56
Cd	0.095	21.35	0.03
Ni	0.068	17.135	0.03
Co	0.042	11.12	0.41

$$q_t = K_i t^{0.5} + C \quad (11)$$

Whereby q_i represents the adsorption capacity (mg/g) at various time intervals, C stands for the intercept (mg/g), and K_i is the rate constant for intraparticle diffusion (mg/g min^{-0.5}) during the occurrence of adsorption. The plot of q_t against $t^{0.5}$ results in a straight line passing through the origin if intraparticle diffusion is the controlling step in the adsorption process. This plot for the Pb, Cd, Ni, and Co ions individually, as seen in Figure 11, showed stepwise-linear patterns with three slopes. The fact that the second slope does not pass through the origin might suggest that intraparticle diffusion is not the

Table 4. Comparison of PAN-MSNs sorption capacities (mg/g) with phenanthroline chelators immobilized on other substrates.

Resin	Metal ions				References
	Cd	Pb	Co	Ni	
PAN -Silica gel	93.06	91.89	[56]
PAN- Amberlite XAD-4*	18.80	48.01	18.01	...	[57]
PAN- Silica monolith*	8.20	8.22	[36]
PAN-MSNs	116	121	130	132	Current work

* The unit was converted from (mM/g) to (mg/g) by multiply by atomic weight of metal.

only step limiting the sorption rate. This could indicate that various other interaction mechanisms, like physical adsorption, intraparticle diffusion, ion exchange, and metal ion complexation with chelator, may also be involved in the sorption of metals.

The sorption capacities of the synthesized PAN-MSNs chelators for the investigated metal ion were compared with various resins incorporating phenanthroline moieties immobilized onto different substrates; silica gel, Amberlite XAD-4, and silica monolith (Table 4). The PAN-MSNs nano-chelating resin exhibited higher sorption capacity. This finding could be ascribed to the high surface area of MSN substrates.

3.3 Application of PCA-MSNs for SPE of metals

The synthesized nano-chelating resin, PCA-MSNs, has been applied to sample pretreatment in a batch manner. This straightforward method, wherein the nano-sorbents distributed in sample solutions, facilitated rapid extraction with high efficiency of recovery [55].

3.3.1. Method recovery

The accuracy of the procedure was evaluated using wastewater reference materials (ERM®-CA713, European Commission, Joint Research Centre (JRC), Geel, Belgium), following the protocol described in the SPE experiments. The standards used for the generation of calibration curves were prepared in a 1% nitric acid aqueous solution, covering the dynamic range presented in Table 5, and exploited to determine the concentration of selected metals in actual samples (ERM®-CA713 reference materials and real samples).

Table 6 presents the concentrations (recovery values) of the metals analyzed in reference materials, together with the certified values. Apparently, all ions in the wastewater reference matrix samples were quantified with satisfactory results.

3.3.2. Analysis of wastewater real samples

The optimized and validated dispersed SPE method using synthesized PCA-MSNs was used to preconcentrate the targeted metal

Table 5. Calibration parameters from buffered standards following dispersed SPE using PCA-MSNs.

Calibration parameter	ions			Pd
	Cd	Co	Ni	
Concentration range ($\mu\text{g/l}$)	Blk-10	Blk-25	Blk-100	Blk-100
Calibration coefficient R^2	0.998	0.999	0.996	0.997
RSD at 2 ngml^{-1} (% n=3)	2.52	1.89	3.21	2.72
Sensitivity, CPS ratio/($\mu\text{g/l}$)	1.51	0.92	0.83	1.13
LOD ($\mu\text{g/l}$)	0.006	0.005	0.009	0.012

Blk: blank

Table 6. Analysis of reference materials, ERM-CA713 wastewater after dispersed SPE using PCA-MSNs for SPE of metals nano resin; results are mean \pm RSD ($\mu\text{g/l}$) and (recovery %).

ions	Found	Certified	Recovery %
Cd	5.1 \pm 0.2	5.2 \pm 0.2	98.07
Pb	50.1 \pm 1.4	49.7 \pm 1.7	100.80
Ni	47.6 \pm 1.5	50.3 \pm 1.4	94.63
Co	nd	nd	nd

Table 7. Concentration of target metal ions in wastewater samples following their preconcentration with SPE.

Concentration of ions ($\mu\text{g/L}$)				
Sample id	Cd	Co	Ni	Pd
IWW	1.3 \pm 0.2	3.7 \pm 1.0	12 \pm 0.8	7.6 \pm 0.5
EPA limit (mg/l)	0.1	na	0.2	0.1
HWW	5 \pm 0.3	13.3 \pm 1.1	13.9 \pm 1.4	10 \pm 0.3
EPA limit (mg/l)	0.1	na	0.2	0.2

IWW: Industrial wastewater, HWW: Hospital wastewater.

ions in treated wastewater real samples collected from King Salman Medical City Treatment Plant (hospital wastewater; coded as HWW and industrial wastewater from Yanbu refinery; coded as IWW). The results are shown in Table 7. The HWW values were lower or comparable to those reported by Amouei *et al.* [58] in wastewater samples collected from Iranian hospitals, and they were all within EPA permitted limits [59]. On the other hand, the concentrations of the analyzed heavy metals in IWW were approximately the same as the results obtained from the effluent of a Nigerian petroleum refinery [60]. In addition, the determined concentrations are within the EPA's permitted limits for this wastewater.

3.3.3. Stability and reusability of PAC-MSNs chelator

The stability and reusability of the PCA-MSNs nano-chelator were evaluated by measuring its sorption capacity after regeneration and treatment with HNO_3 (up to 5 M) and ammonium hydroxide (up to pH 10), as well as after 10 application cycles [61]. It was found that the sorption capacity of the chelator regenerated with nitric acid (1–4 M) was comparable to that of the new material, with a variation of $\leq 1.8\%$. This indicates that the resin can withstand up to 4.0 M HNO_3 . However, when exposed to a stronger acid (5.0 M HNO_3), a light greenish-yellow coloration was immediately observed in the acid solution. This is likely due to the cleavage of the ether group in the aminophenoxypropyl linker arm under highly concentrated acidic conditions, which also led to a significant reduction in sorption capacity ($\geq 4.6\%$).

Similarly, when the material was immersed in an alkaline solution with pH >10 , discoloration occurred in the solution, and the sorption capacity decreased by 3.8%. The sorption capacity for the studied metal ions was further assessed after repeated loading and elution cycles. An insignificant decrease in capacity (2.41%) was observed after approximately 15 cycles, demonstrating the material's durability.

In addition, when stored in a desiccator for 10 months, the sorption capacity of the PCA-MSNs nano-chelator did not show any significant changes. Therefore, the chelating resin is highly stable and reusable for extended periods and multiple applications.

4. Conclusions

The present work demonstrates the feasibility of using cost-effective, high-surface-area MSNs synthesized via a simple hydrothermal-assisted sol-gel method from sodium silicate solutions as a substrate for the immobilization of PCA moiety. The straightforward chemical modification allowed the successful synthesis of an efficient PCA-MSNs nano-chelating resin, appropriate for the extraction of transition metals from aqueous bodies.

TGA and FTIR provided strong evidence confirming the successful grafting of PCA chelating agents onto the MSNs. The PCA-MSNs demonstrated significantly enhanced sorption capacity for the extraction of Pb, Cd, Ni, and Co ions from aqueous solutions compared to resins containing the same chelating center. The adsorption efficiency was found to be highly dependent on the pH of the solution, reflecting the pH-sensitive nature of the chelation process.

Kinetic studies revealed that the adsorption behavior closely followed the pseudo-second-order kinetics model, while the adsorption isotherms were best described by the Langmuir model. Furthermore, the intraparticle diffusion analysis suggested that the diffusion rate was influenced by complex formation chemical reactions involved in the chelation process.

The novel nano-sorbent, PCA-MSNs, demonstrated excellent performance as a specific and effective sorbent for extracting Pb, Cd, Ni, and Co ions from water matrices. This efficiency can be attributed to the chelating resin's optimized structural organization, high surface area, and significant porosity, which facilitate access to the immobilized chelating groups within the mesoporous framework. The successful application of PCA-MSNs as selective extraction sorbent for the targeted ions from wastewater matrices highlights its potential applications for the removal of heavy/transition metal ions in wastewater treatment processes.

CRedit authorship contribution statement

A.O. AlSuhaimi. and H.M. Albishri: Proposed project and developed methodology, K.M. AlMuhaimadi., B.H.M. Hussein., A.O. AlSuhaimi., and K.A. AlThuyiri: Synthesized and applied of materials, A.O. AlSuhaimi., B.H.M. Hussein., K.M. AlMuhaimadi. and K.A. AlThuyiri: Prepared and wrote the original draft, B.H.M. Hussein., A.O. AlSuhaimi: Reviewed and edited the manuscript. All authors have read and agreed to the published version of the manuscript.

Declaration of competing interest

The authors declare no conflicts of interest.

Declaration of Generative AI and AI-assisted technologies in the writing process

The authors confirm that there was no use of AI-assisted technology for assisting in the writing of the manuscript and no images were manipulated using AI.

References

1. Camel, V., 2003. Solid phase extraction of trace elements. *Spectrochimica Acta Part B: Atomic Spectroscopy* **58**, 1177–1233. [https://doi.org/10.1016/S0584-8547\(03\)00072-7](https://doi.org/10.1016/S0584-8547(03)00072-7)
2. Velarde, L., Nabavi, M.S., Escalera, E., Antti, M.-L., Akhtar, F., 2023. Adsorption of heavy metals on natural zeolites: A review. *Chemosphere* **328**, 138508. <https://doi.org/10.1016/j.chemosphere.2023.138508>
3. Dimpe, K.M., Ngila, J.C., Nomngongo, P.N., 2018. Preparation and application of a tyre-based activated carbon solid phase extraction of heavy metals in wastewater samples. *Physics and Chemistry of the Earth, Parts A/B/C* **105**, 161–169. <https://doi.org/10.1016/j.pce.2018.02.005>
4. Azarova, Yu.A., Pestov, A.V., Bratskaya, S.Yu., 2016. Application of chitosan and its derivatives for solid-phase extraction of metal and metalloids ions: a mini-review. *Cell* **23**, 2273–2289. <https://doi.org/10.1007/s10570-016-0962-6>
5. Mousavi, S.E., Kalal, H.S., Ghorbanian, S.A., Khamseh, A.A.G., Khanchi, A.R., 2023. A comparison of various XAD-Amberlite resins impregnated with dicyclohexyl-18-crown-6 for strontium removal. *Progress in Nuclear Energy* **166**, 104965–104965. <https://doi.org/10.1016/j.pnucene.2023.104965>

6. Omer, O.S., Hussein, B.H.M., Hussein, M.A., Mgaidi, A., 2017. Mixture of illite-kaolinite for efficient water purification: Removal of As(III) from aqueous solutions. *Desal Water Treat* **79**, 273–281. <https://doi.org/10.5004/dwt.2017.20801>
7. Omer, O.S., Hussein, B.H.M., Ouf, A.M., Hussein, M.A., Mgaidi, A., 2018. An organified mixture of illite-kaolinite for the removal of Congo red from wastewater. *Journal of Taibah University Medical Sciences* **12**, 858–866. <https://doi.org/10.1080/16583655.2018.1540179>
8. Querol, X., Alastuey, A., Moreno, N., Alvarez-Ayuso, E., García-Sánchez, A., Cama, J., Avora, C., Simón, M., 2006. Immobilization of heavy metals in polluted soils by the addition of zeolitic material synthesized from coal fly ash. *Chemosphere* **62**, 171–180. <https://doi.org/10.1016/j.chemosphere.2005.05.029>
9. Kumar, R., Rauwel, P., Rauwel, E., 2021. Nanoadsorbents for the removal of heavy metals from contaminated water: Current scenario and future directions. *Processes* **9**, 1379. <https://doi.org/10.3390/pr9081379>
10. Ethaib, S., Al-Qutaifa, S., Al-Ansari, N., Zubaidi, S.L., 2022. Function of nanomaterials in removing heavy metals for water and wastewater remediation: A Review. *Environmental* **9**, 123. <https://doi.org/10.3390/environments9100123>
11. Arun Karnwal, Malik, T., 2024. Nano-revolution in heavy metal removal: engineered nanomaterials for cleaner water. *Frontiers Environmental Science* **12**. <https://doi.org/10.3389/fenvs.2024.1393694>
12. Xie, L., Jiang, R., Zhu, F., Liu, H., Ouyang, G., 2013. Application of functionalized magnetic nanoparticles in sample preparation. *Analytical and Bioanalytical Chemistry* **406**, 377–399. <https://doi.org/10.1007/s00216-013-7302-6>
13. Khan, W.A., Arain, M.B., Soyak, M., 2020. Nanomaterials-based solid phase extraction and solid phase microextraction for heavy metals food toxicity. *Food and Chemical Toxicology*, **145**, 111704. <https://doi.org/10.1016/j.fct.2020.111704>
14. Yang, X., Zhou, B., Wang, C., Tan, R., Cheng, S., Saleem, A., Zhang, Y., 2023. Mesoporous silica nanoparticles for the uptake of toxic antimony from aqueous matrices. *ACS Omega* **8**, 26916–26925. <https://doi.org/10.1021/acsomega.3c01735>
15. Wang, B., Zhou, Y., Li, L., Xu, H., Sun, Y., Wang, Y., 2018. Novel synthesis of cyano-functionalized mesoporous silica nanospheres (MSN) from coal fly ash for removal of toxic metals from wastewater. *Journal of Hazardous Materials* **345**, 76–86.
16. Ścigalski, P.; Kosobucki, P., 2020. Recent Materials Developed for Dispersive Solid Phase Extraction. *Molecules* **25**, 4869. <https://doi.org/10.3390/molecules25214869>
17. Fowler, C.E., Khushalani, D., Lebeau, B., Mann, S., 2001. Nanoscale materials with mesostructured interiors. *Advanced Materials* **13**, 649–652. [https://doi.org/10.1002/1521-4095\(200105\)13:9<649::AID-ADMA649>3.0.CO;2-G](https://doi.org/10.1002/1521-4095(200105)13:9<649::AID-ADMA649>3.0.CO;2-G)
18. Suzuki, K., Ikari, K., Imai, H., 2003. Synthesis of silica nanoparticles having a well-ordered mesostructure using a double surfactant system. *Journal of the American Chemical Society* **126**, 462–463. <https://doi.org/10.1021/ja038250d>
19. Qiao, Z.-A., Zhang, L., Guo, M., Liu, Y., Huo, Q., 2009. Synthesis of mesoporous silica nanoparticles via controlled hydrolysis and condensation of silicon alkoxide. *Chemistry of Materials* **21**, 3823–3829. <https://doi.org/10.1021/cm901335k>
20. Wu, S.-H., Mou, C.-Y., Lin, H.-P., 2013. Synthesis of mesoporous silica nanoparticles. *Chemical Society Reviews* **42**, 3862. <https://doi.org/10.1039/C3CS35405A>
21. Karande, S.D., Jadhav, S.A., Garud, H.B., Kalantre, V.A., Burungale, S.H., Patil, P.S., 2021. Green and sustainable synthesis of silica nanoparticles. *Nanotechnology for Environmental Engineering* **6**, <https://doi.org/10.1007/s41204-021-00124-1>
22. Nooney, R.L., Thirunavukkarasu, D., Chen, Y., Josephs, R., Ostafin, A.E., 2002. Synthesis of nanoscale mesoporous silica spheres with controlled particle size. *Chemistry of Materials* **14**, 4721–4728. <https://doi.org/10.1021/cm0204371>
23. Kosuge, K., Kikukawa, N., Takemori, M., 2004. One-step preparation of porous silica spheres from sodium silicate using triblock copolymer templating. *Chemistry of Materials* **16**, 4181–4186.
24. Hwang, J., Lee, J.H., Chun, J., 2021. Facile approach for the synthesis of spherical mesoporous silica nanoparticles from sodium silicate. *Materials Letters* **283**, 128765. <https://doi.org/10.1016/j.matlet.2020.128765>
25. Gu, L., Zhang, A., Hou, K., Dai, C., Zhang, S., Liu, M., Song, C., Guo, X., 2012. One-pot hydrothermal synthesis of mesoporous silica nanoparticles using formaldehyde as growth suppressant. *Microporous and Mesoporous Materials* **152**, 9–15. <https://doi.org/10.1016/j.micromeso.2011.11.047>
26. Meléndez-Ortiz, H.I., Mercado-Silva, A., García-Cerda L. A., Castruita, G., Perera-Mercado Y.A., 2017. Hydrothermal synthesis of mesoporous silica MCM-41 Using Commercial Sodium Silicate. *Journal of the Mexican Chemical Society*. **57**(2), 73-79. <https://doi.org/10.29356/jmcs.v57i2.215>
27. Purwaningsih, H., Pratiwi, V.M., Purwana, S.A.B., Nurdiansyah, H., Rahmawati, Y., Susanti, D., 2018. Fabrication of mesoporous silica nanoparticles by sol gel method followed various hydrothermal temperature. *AIP Conference Proceedings* **1945**, 020052. <https://doi.org/10.1063/1.5030274>
28. Huang, C., Hu, B., 2008. Silica-coated magnetic nanoparticles modified with γ -mercaptopropyltrimethoxysilane for fast and selective solid phase extraction of trace amounts of Cd, Cu, Hg, and Pb in environmental and biological samples prior to their determination by inductively coupled plasma mass spectrometry. *Spectrochim. Acta Part B: Atomic Spectroscopy* **63**, 437–444. <https://doi.org/10.1016/j.sab.2007.12.010>
29. Shishchbore, M.R., Afkhami, A., Bagheri, H., 2011. Salicylic acid functionalized silica-coated magnetite nanoparticles for solid phase extraction and preconcentration of some heavy metal ions from various real samples. *Chemistry Central Journal* **5**. <https://doi.org/10.1186/1752-153X-5-41>
30. Rajabi, M., Barfi, B., Asghari, A., Najafi, F., Aran, R., 2014. Hybrid amine-functionalized titania/silica nanoparticles for solid-phase extraction of lead, copper, and zinc from food and water samples: Kinetics and equilibrium studies. *Food Analytical Methods* **8**, 815–824. <https://doi.org/10.1007/s12161-014-9964-x>
31. Shirkanloo, H., Falahnejad, M., Zavvar Mousavi, H., 2015. On-line ultrasound-assisted dispersive micro-solid-phase extraction based on amino bimodal mesoporous silica nanoparticles for the preconcentration and determination of cadmium in human biological samples. *Biological Trace Element Research* **171**, 472–481. <https://doi.org/10.1007/s12011-015-0538-6>
32. Davari, S., Hosseini, F., Shirkanloo, H., 2018. Dispersive solid phase microextraction based on aminefunctionalized bimodal mesoporous silica nanoparticles for separation and determination of calcium ions in chronic kidney disease. *Analytical Methods in Environmental Chemistry Journal* **1**, 57–66. <https://doi.org/10.24200/amec.v1.i01.37>
33. Kazemi, M., 2017. Solid phase extraction based on thiol functionalized magnetite nanoparticles to determination some heavy metal ions in water samples using atomic absorption spectrometry. *Current Analytical Chemistry* **13**, 174–180. <https://doi.org/10.2174/1573411012666160504124118>
34. Al-Wasidi, A.S., Katouah, H.A., Saad, F.A., Abdelrahman, E.A., 2023. Functionalization of silica nanoparticles by 5-Chloro-8-quinolinol as a new nanocomposite for the efficient removal and preconcentration of Al³⁺ ions from water samples. *ACS Omega* **8**, 15276–15287. <https://doi.org/10.1021/acsomega.3c00413>
35. Bencini, A., Lippolis, V., 2010. 1,10-Phenanthroline: A versatile building block for the construction of ligands for various purposes. *Coordination Chemistry Reviews* **254**, 2096–2180. <https://doi.org/10.1016/j.ccr.2010.04.008>
36. ALSuhaimi, A.O., AlMohaimadi, Khaled M., AlAlawi, B.N., Ali, I., 2018. A novel porous silica monolith functionalized with 5-amino-1,10-phenanthroline for SPE of metal ions in groundwater samples prior to their analysis using ICP-MS. *Analytical Methods* **10**, 2337–2346. <https://doi.org/10.1039/c8ay00442k>
37. AlMohaimadi, K.M., Albishri, H.M., Thumayri, K.A., ALSuhaimi, A.O., Mehdar, Y.T., Hussein, B.H., 2024. Facile Hydrothermal Assisted Basic Catalyzed Sol Gel Synthesis for Mesoporous Silica Nanoparticle from Alkali Silicate Solutions using Dual Structural Templates. *Gels* **10**, 839. <https://doi.org/10.3390/gels10120839>
38. Bagwe, R.P., Hilliard, L.R., Tan, W., 2006. Surface modification of silica nanoparticles to reduce aggregation and nonspecific binding. *Langmuir* **22**, 4357–4362. <https://doi.org/10.1021/la052797j>
39. Muroya M. A., 1999. Correlation between the formation of silica skeleton structure and Fourier transform infrared absorption spectroscopy spectra. *Colloids and Surfaces A: Physicochemical and Engineering* **157**, 147–155. [https://doi.org/10.1016/S0927-7757\(99\)00054-0](https://doi.org/10.1016/S0927-7757(99)00054-0)
40. Morrow, B.A., Molapo, D.T., 2006. Infrared studies of chemically modified silica, in: *Colloidal Silica: Fundamentals and Applications*. Taylor & Francis Group, pp. 212–319. <https://research.sabanciuniv.edu/id/eprint/36587>
41. Lu, H.-T., 2013. Synthesis and characterization of amino-functionalized silica nanoparticles. *Russian Journal of Earth Sciences* **75**, 343–350. <https://doi.org/10.7868/s0023291213030130>
42. Rahman, N.A., Widhiana, I., Juliastuti, S.R., Setyawan, H., 2015. Synthesis of mesoporous silica with controlled pore structure from bagasse ash as a silica source. *Colloids and Surfaces A: Physicochemical and Engineering* **476**, 1–7. <https://doi.org/10.1016/j.colsurfa.2015.03.018>
43. Gorbunova O. V., Baklanova O.N., Gulyaeva T.I., 2020. Porous structure of PEG-mediated silica controlled by solution pH. *Microporous and Mesoporous Materials* **307**, 110468–110468. <https://doi.org/10.1016/j.micromeso.2020.110468>
44. ALSuhaimi, A.O., AlRadaddi, S.M., Ali, Shraim, A.M., AlRadaddi, T.S., 2019. Silica-based chelating resin bearing dual 8-Hydroxyquinoline moieties and its applications for solid phase extraction of trace metals from seawater prior to their analysis by ICP-MS. *Arabian Journal of Chemistry* **12**, 360–369. <https://doi.org/10.1016/j.arabjc.2017.10.006>
45. Langmuir, I., 1916. The constitution and fundamental properties of solids and liquids. *J Am Chem Soc*. **38**, 2221–2295. <https://doi.org/10.1021/ja02268a002>
46. Freundlich, H., 1907. Über die adsorption in lösungen. *Journal of Physical Chemistry* **57**, 1907-5723. <https://doi.org/10.1515/zpch-1907-5723>
47. Ho, Y.S., McKay, G., 1998. Kinetic model for lead(II) sorption on to peat. *Adsorption Science & Technology* **16**, 243–255. <https://doi.org/10.1177/026361749801600401>
48. Aksu, Z., 2002. Determination of the equilibrium, kinetic and thermodynamic parameters of the batch biosorption of nickel(II) ions onto chlorella vulgaris. *Process Biochemistry* **38**, 89–99. [https://doi.org/10.1016/S0032-9592\(02\)00051-1](https://doi.org/10.1016/S0032-9592(02)00051-1)
49. Tan, L., Xu, J., Xue, X., Lou, Z., Zhu, J., Baig, S.A., Xu, X., 2014. Multifunctional nanocomposite Fe₃O₄@SiO₂-mPD/SP for selective removal of Pb(II) and Cr(VI) from aqueous solutions. *RSC Advances* **4**, 45920–45929. <https://doi.org/10.1039/c4ra08040h>
50. Lagergren, S., 1898. Zur Theorie der sogenannten adsorption gelöster stoffe. *Kungliga Svenska Vetenskapsakademiens Handlingar* **24**, 1–39.
51. Ho, Y.S., McKay, G., 1999. Pseudo-second order model for sorption processes. *Process Biochemistry* **34**, 451–465. [https://doi.org/10.1016/S0032-9592\(98\)00112-5](https://doi.org/10.1016/S0032-9592(98)00112-5)
52. Zargoosh, K., Zilouei, H., Mohammadi, M.R., Abedini, H., 2014. 4-Phenyl-3-thiosemicarbazide modified magnetic nanoparticles: Synthesis, characterization and application for heavy metal removal. *CLEAN-Soil Air Water* **42**, 1208–1215. <https://doi.org/10.1002/clen.201300524>
53. Yang, G., Tang, L., Cai, Y., Zeng, G., Guo, P., Chen, G., Zhou, Y., Tang, J., Chen, J., Weiping Xiong, W., 2014. Effective removal of Cr(VI) through adsorption and reduction by magnetic mesoporous carbon incorporated with polyaniline. *RSC Advances* **4**, 58362–58371. <https://doi.org/10.1039/c4ra08432b>
54. Zhu, X., Chen, B., Zhu, L., Xing, B., 2017. Effects and mechanisms of biochar-microbe interactions in soil improvement and pollution remediation: A review. *Envir. Poll* **227**, 98–115. <https://doi.org/10.1016/j.envpol.2017.04.032>
55. Bauer, G., Neouze, M.-A., Limbeck, A., 2013. Dispersed particle extraction—A new procedure for trace element enrichment from natural aqueous samples with subsequent ICP-OES analysis. *Talanta* **103**, 145–152. <https://doi.org/10.1016/j.talanta.2012.10.023>
56. Giron, O.D., Lirag, R.C.M., Arco, S.D., Quirit, L.L., 2013. Modification of silica gel with 1,10-Phenanthroline for Cd(II) and Pb(II) adsorption. *KIMIKA* **24**, 18–24. <https://doi.org/10.26534/kimika.v24i1.18-24>

57. Hashemi-Moghaddam, H., Haghiri, H.K., 2014. Preconcentration of some heavy metals by Amberlite XAD-4 functionalized with phenanthroline and investigation of microwave radiation effect on kinetic of adsorption. *Desalination and Water Treatment* 57, 1705–1712. <https://doi.org/10.1080/19443994.2014.976766>
58. Amouei, A., Asgharnia, H., Fallah, H., Faraji, H., Barari, R., Naghipour, D., 2015. Characteristics of effluent wastewater in hospitals of babol university of medical sciences, Babol, *Iranian Journal of Health Sciences* 4, e23222. <https://doi.org/10.17795/jhealthscope-23222>
59. US EPA,OW, 2014. Effluent Guidelines | US EPA [WWW Document]. US EPA. accessed at (<https://www.epa.gov/eg> on 23/10/2024)
60. Uzoekwe, S.A., Oghosanine, F.A., 2011. The Effect of refinery and petrochemical effluent on water quality of Ubeji Creek Warri, Southern Nigeria. *Ethiopian Journal of Environmental Studies and Management* 4, <https://doi.org/10.4314/ejesm.v4i2.12>
61. ALSuhaimi, A. O., Mccreedy, T., 2013. Rapid immobilisation of 8-hydroxyquinoline onto silica materials and its application for on-line solid-phase extraction of transition metals from environmental samples before ICP-OES monitoring. *Global NEST Journal* 14, 55–65. <https://doi.org/10.30955/gnj.000817>